ACS APPLIED ELECTRONIC MATERIALS

pubs.acs.org/acsaelm Article

Power-Level Electrical Switch Enabled by a Liquid-Metal Bridge

Xiaonan Zhu, Fei Yang,* Haoran Wang, Siyuan Zhao, Yi Wu, Shi-Yang Tang,* and Mingzhe Rong*

Cite This: *ACS Appl. Electron. Mater.* 2022, 4, 2859−2868 Read Online

ACCESS | Metrics & More | Article Recommendations | Supporting Information

ABSTRACT: Soft electronic components possess the potential to be developed into next-generation electrical devices that can provide superior performance to solid-state counterparts. Among commonly used components, electrical switches are an essential control element in electrical and electronic systems. Both solid-state mechanical and semiconductor switches are blamed for some intrinsic shortcomings. For example, the former suffers from contact surface degradation, while the latter functions with a high conduction loss. To overcome the limitations, here, a liquid metal (LM)-enabled electrical switch is reported by incorporating a Galinstan liquid bridge into a pair of solid electrodes. The electrical switch operation is realized by the coalescence of LM droplets and the breakup of the LM bridge. Extraordinarily, the device is capable of interrupting a DC 220 V, 1−5 A circuit within 11 ms, outperforming a common mechanical switch by a factor of 4−20 in terms of interruption speed. During the breakup process of an LM bridge in the presence of a current, three regimes characterized by electrical arc behaviors are identified and investigated. The rupture distance formed before pinch-off is critical to regulate the arc plasma behaviors. The presented applications and discoveries have a vast potential in both practical technologies, involving high-current electrical and electronic equipment, and fundamental research fields relevant to soft electronics, fluid mechanics, and plasma science.

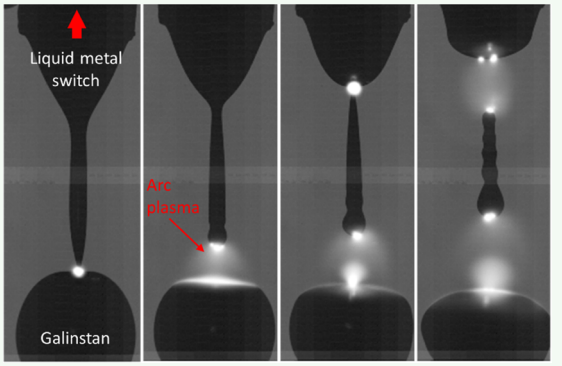

KEYWORDS: *liquid metal, Galinstan, liquid bridge, electrical switch, soft electrical components*

1. INTRODUCTION

The emerging boom of soft electronics is bringing tremendous revolutions and great convenience to fields such as human healthcare monitoring, sports science, energy harvesting, and human−machine interface.[1−6] For all of the above electronic and electrical systems, one of the most fundamental elements is electrical switch. It is indispensable in a wide range of occasions involving electric circuits for either signal[7] or power transmission.[8] The long history of the development of switching technologies breeds two main members in the electrical switch family—the mechanical switch and the semiconductor switch, both of which are in a solid state. Although considerable progress has been achieved in solid conductor-based soft electronics,[9] the existence of the solid-state switch may cause the collapse of a soft electronic system due to the incompatible mechanical flexibility and stretchability.

Moreover, some intrinsic shortcomings caused by solid-state conduction have always been the bottleneck for switch devices. Essential parts of a mechanical switch contain a pair of electrical contacts made of solid metals or their oxides with superior electrical properties, such as silver metal oxides[10] and silver refractory metals.[11] The existence of the solid contact makes it possible to achieve both a low contact resistance (<50 mΩ) in the on-state and a very high isolation impedance (10^{10}−10^{14} Ω) in the off-state.[7] However, due to its intrinsic rigidity, solid contacts cause several inevitable issues during operation, including contact bounce, mechanical wear, surface erosion, and welding.[7] Ren et al. conducted comprehensive and explicit research toward degradation problems of rated power used electrical contacts in regard to mechanical, electrical, and environment factors.[12,13] These shortcomings limit the reliability and lifetimes of mechanical switching devices. Alternatively, the semiconductor switch, which realizes current switching relying on transistors or thyristors, avoids arc plasma and thus contact degradation when interrupting high currents. Nevertheless, these devices result in large conduction losses and a low on−off impedance ratio because they are not pure conductors, resulting in a high on-state resistance as well as a leakage current under off condition.[14] Therefore, an electrical switching element concurrently possesses infinite deformability, power-level current handling ability, self-healing of contact surfaces, a low conduction resistance, and a high switching impedance ratio, is ideal and may revolutionize the development of future electrical switches.

Received: March 18, 2022
Accepted: May 17, 2022
Published: June 1, 2022

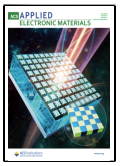

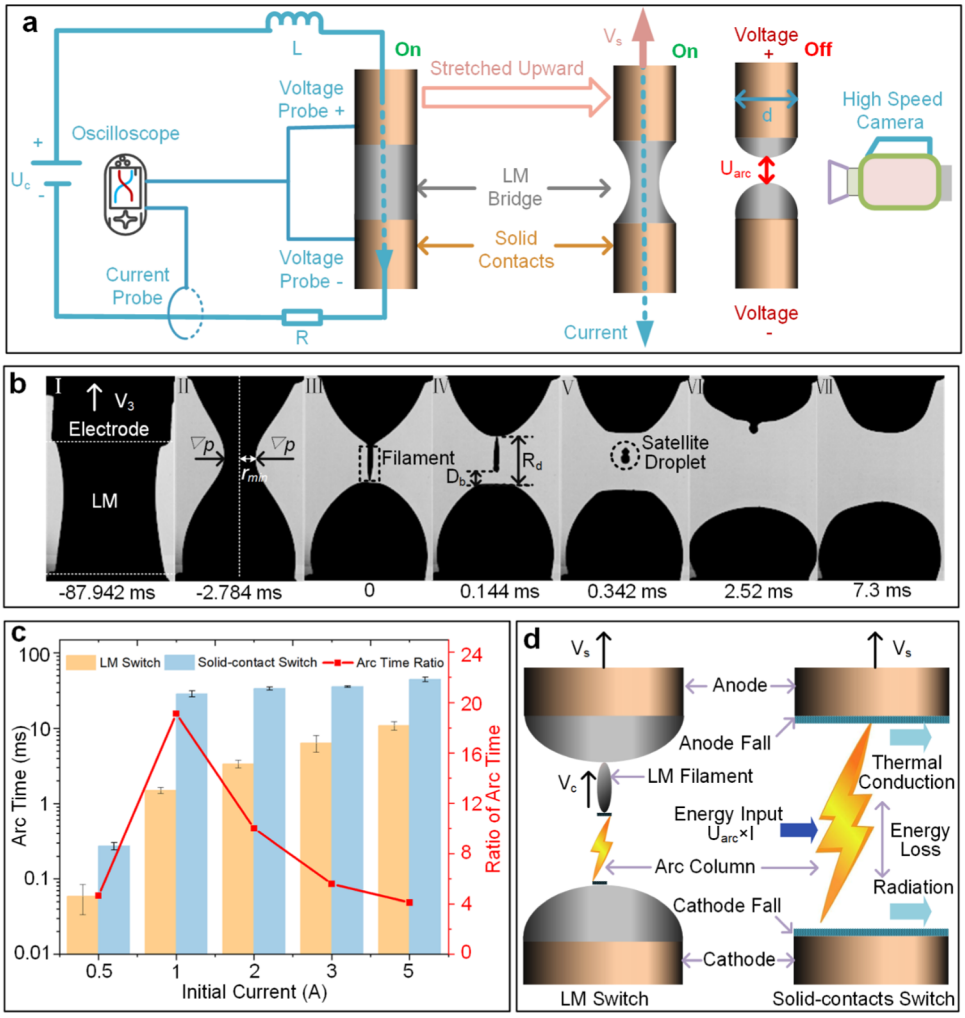

Figure 1. Concept and working performance of the LM bridge-enabled electrical switch. (a) Concept design and experiment schematic of the LM switch. (b) Series of snapshots depicting the capillary breakup process of an LM bridge switch. The image sequences are captured by a high-speed camera at a sampling rate of 166 172 frames per second with a 1.2 μs exposure time; t = 0 is set at the first breakpoint of the filament. (c) Comparison of LM and solid contact switches' arc time at different initial currents. The arc time is measured from current and voltage waveforms captured by an oscilloscope. Every arc time is averaged by three consecutive experimental results under the same parameters, and the error bars represent the standard deviation. (d) Working mechanism of LM and solid contact switches: stretching electrical arc to interrupt current.

Liquid bridge is an intriguing and delicate phenomenon enabled by the surface tension of fluids. The ubiquitous natural scene has motivated researchers to utilize it in diverse industrial applications such as particle[15] and hydrogel fabrication,[16] ink-jet printing,[17] switchable adhesion,[18] and optical micro-lenses.[19] Endowed with the largest surface tensions (>500 mN/m) at room temperature[20] among typical liquids, gallium-based liquid metals (LM) could induce a much more dramatic bridge breakup process. Coupled with a high electrical conductivity, the morphological transformation between droplets coalescence and liquid bridge breakup could be naturally regarded as an electrical switching process. Inspired by the good electrical conductivity of LM ($\sim 3 \times 10^6$ S/m),[21] self-healing ability originated from liquidity, and a high-speed liquid bridge breakup caused by a large surface tension, we expect a controllable LM bridge to be an attractive choice for realizing ideal electrical switches. From the same point of view, a field control electrical switch based on electrochemistry-induced coalescence and breakup of LM droplets has been designed,[22] while the on−off ratio and current handing level of the device have been restricted by the conductive NaOH solution. Some of the previous works in our group concentrate on an LM current limiter, which exploits high electromagnetic pinch force to break an LM conductive channel and ignite electrical arc.[23,24] To realize a sufficient drive of the conductive LM channel, the current limiter requires an extremely high current amplitude at the kiloampere level, which means it is only applicable to transient short-circuit current application. To date, LM-based electrical switch suitable for rated power application has not been well developed.

Here, a room-temperature LM, Galinstan (68.5% gallium, 21.5% indium, and 10% tin),[25] is used as a core part to construct a power-level electrical switch based on the formation and breakup of a LM capillary bridge. We particularly pay attention to its current interruption capability as power equipment. Arc plasma behaviors and LM bridge dynamics during current interruptions are characterized in our investigation. In this way, implied theories and regulation strategies for the switch's characteristics are formulated.

https://doi.org/10.1021/acsaelm.2c00352
ACS Appl. Electron. Mater. 2022, 4, 2859−2868

2. RESULTS AND DISCUSSION

Figure 1a describes the concept of a LM bridge-enabled electrical switch and the testing experiment scheme. To build the switch prototype, two Galinstan droplets are deposited on a pair of solid contacts (diameter d of 3 mm), of which the surfaces are tinned to enhance an excellent wetting between LM and solid electrodes. When moving the upper electrode with an LM droplet attached downward, two LM droplets coalesce to form a conductive bridge, allowing the electric current to flow to switch on a circuit. By contrast, when the upper electrode is upward-driven, the LM bridge will be stretched to deform and induce a capillary breakup at the stability limit.[26] Finally, the liquid bridge breaks into two separated hemispherical droplets and switches off the circuit. By adjusting the driving current of the electromagnetic mechanism equipped in the switch prototype, we can get three typical motion characteristic curves of the upper electrode. Correspondingly, the upper surface of the LM bridge moves up with three distinct stretching velocities and we define them as high speed V_1 (0.4 m/s in average), middle speed V_2 (0.1 m/s in average), and low speed V_3 (0.024 m/s in average). Mainly depending on an oscilloscope and a high-speed camera, electrical measurement and visualization of the switching process are combined to characterize the switch's performance and elaborate the working mechanism. As soon as Galinstan is exposed to ambient air, its surface gets oxidized instantaneously.[27] As discovered in previous works,[28−30] the existence of an oxide skin lowers the surface tension, increases the yield stress of Galinstan/EGaIn, and makes it easier to adhere to many surfaces. Consequently, the LM will be stabilized and behave more like a solid material. For an electrical switch, the existence of an oxide skin inhibits the capillary breakup process by lowering the interfacial tension and increasing the yield stress of Galinstan, which is detrimental to a high-speed switch process. To avoid oxidation, the experimental prototype is operated in a specifically designed glovebox and the N_2 atmosphere in the glovebox is proved to be effective in protecting Galinstan from oxidation. More details about the prototype and the experimental system could be found in Figures S1−S3.

Figure 1b presents the capillary breakup process of a 13 μL LM bridge carrying a 0.1 A current (also see Movie S1). With such a low current, no electrical arc appears during the breakup of the LM bridge. Initially, a stable LM bridge is held by two electrodes due to the wetting of Galinstan to the tinned surface (Figure 1b(I)). The circuit is switched on with an initial current flowing through the LM bridge contact. With the upper electrode moving upward at a low velocity V_3, the LM bridge is first stretched (Figure 1b(II)). At this point, a neck is formed at the waist of the bridge as a result of interfacial tension acting to minimize the surface area.[31] The existence of the neck causes additional pressure on the concave interface, which is called the Laplace pressure. The Laplace pressure, perpendicular to the interface and pointing inward from outward, could be expressed as

$$\Delta p = \sigma(1/R_1 + 1/R_2) = \sigma\kappa \tag{1}$$

where σ is the interfacial tension, R_1 and R_2 are the principal radii of curvature, and κ is (twice) the mean curvature.[31] Obviously, the biggest Laplace pressure is built at the neck point with the thinnest radius of r_{min} and could be formulated as

$$\Delta p = \sigma/r_{min} \tag{2}$$

As the bridge radius decreases under the action of Laplace pressure, the curvature becomes larger at the neck, which in turn further increases the pressure. As a result, LM is expelled with an increasing velocity from the neck.[32] Consequently, a thin filament will form to connect primary droplets with an extremely high Laplace pressure developed at the two ends of the filament (Figure 1b(III)). Owing to gravity, the pressure built at the lower end is much higher than the other and the filament will first pinch off at the lower end. At the same time, the circuit is also switched off within several microseconds (see Supporting information Figure S4 for voltage and current waveforms). Next, with continuous stretching, the filament will pinch off at the higher end and detach from the primary droplet (Figure 1b(IV)). Then, the capillary breakup process is completed. Here, we define the distance between the two primary droplets as the "rupture distance" (R_d) and the distance between the filament tip and the lower primary droplet as the "bottom distance" (D_b) (see Figure 1b(IV)). The detached filament contracts into a satellite droplet, and subsequently, the satellite droplet will oscillate between two primary droplets (Figure 1b(V)) and finally be absorbed by one of the primary droplets (Figure 1b(VI)). We discuss strategies for diminishing the satellite droplets in Figure S5 and give the current interruption process without a satellite droplet in Figure S6. After several cycles of oscillation to dissipate energy (Figure 1b(VII)), two separated droplets will reach a steady state and the whole dynamic process is completed, leaving a large air gap formed between LM droplets to endure applied system voltages.

For a power electrical switch, the harsh challenge lies in its ability to deal with intense electrical discharge and arc plasma burning during the current interruption process. Therefore, switch-off time with the presence of arc plasma is the most critical parameter to judge its interruption capability, and minimizing it is a key to improve the equipment's operating life. To evaluate the performance of the LM switch prototype, power-level current interruption tests are carried out in a DC 220 V circuit, as depicted in Figure 1a. For comparison, a solid-contact switch is also tested under identical conditions (see Supporting information Figure S7 for results summary of the solid-contact switch). The solid-contact switch is a replica of the LM switch prototype (Supporting information Figure S1a) except that no LM bridge is used to wet the solid electrodes. In fact, it is a typical experimental model of conventional mechanical switches. As shown in Figure 1c, the arc time of two types of switches both increases with the increase in initial current, and the developed LM bridge switch outperforms the conventional mechanical switch by a factor of 4−20 in terms of the switch-off time. The general superior performance of the LM switch could be explained as follows. For the DC circuit shown in Figure 1a, which remains to be interrupted with the presence of arc plasma, the Kirchhoff's voltage law is written as

$$U_c = RI + L\frac{dI}{dt} + U_{arc} \Rightarrow \frac{dI}{dt} = \frac{1}{L}[(U_c - RI) - U_{arc}] \tag{3}$$

where I is the circuit current changing with time t; L and R are, respectively, the inductance and the resistivity of the circuit; U_c is the power supply voltage; and U_{arc} is the arc voltage across opened contacts.

https://doi.org/10.1021/acsaelm.2c00352
ACS Appl. Electron. Mater. 2022, 4, 2859−2868

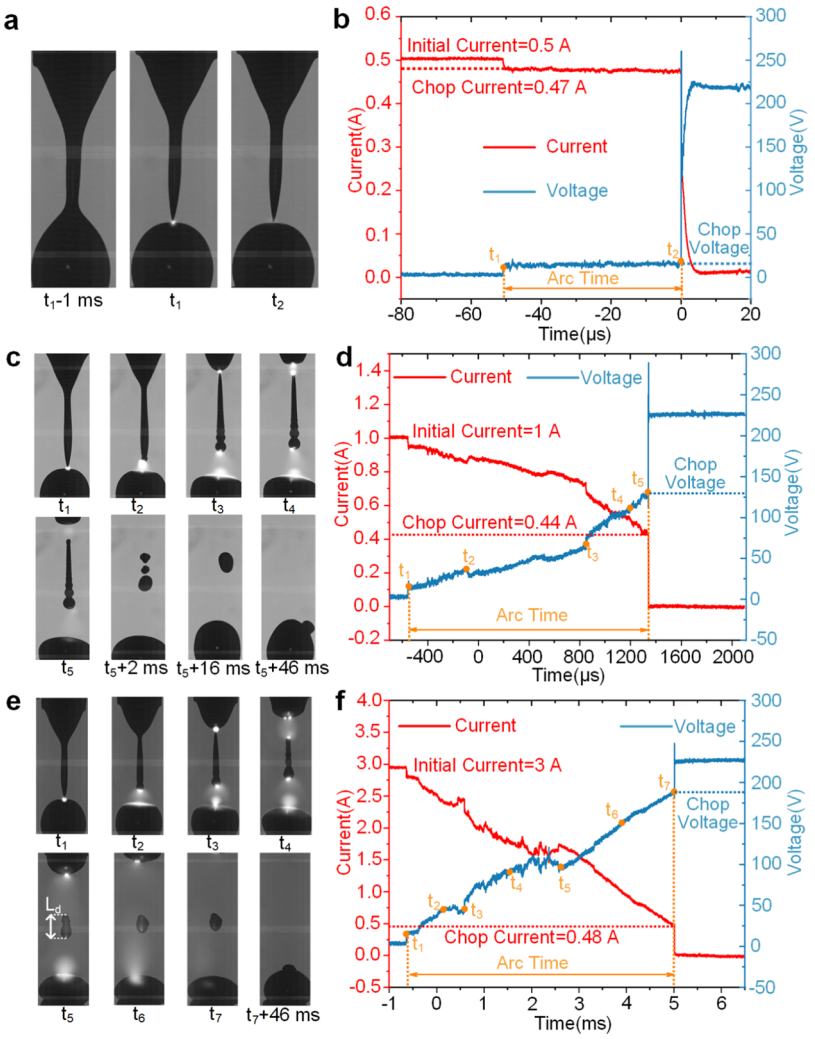

Figure 2. Three regimes describing electrical arc behaviors in the capillary breakup of an LM bridge. (a) Image sequences that depict arc behaviors in regime A. Images are captured at 166 172 fps with a 2.5 μs exposure time. (b) Voltage and current variations of the LM bridge arc during regime A. (c) Image sequences that depict arc behaviors in regime B. Images are captured at 166 667 fps with a 2 μs exposure time. (d) Voltage and current variations of the LM bridge arc during regime B. (e) Image sequences that depict arc behaviors in regime C. Images are captured at 166 667 fps with a 1.4 μs exposure time. (f) Voltage and current variations of the LM bridge arc during regime C. Time points marked as t_n in (a) and (b), (c) and (d), and (e) and (f) correspond to each other.

The arc voltage U_{arc}, as shown in Figure 1d, is composed of a pair of voltage drops in the cathode and anode fall regions as well as the main voltage drop through the arc column.[33] The cathode fall and anode fall are built over a short distance from the opened contact surfaces. They are characterized by extremely high electrical fields, which could be utilized to produce the discharge sustaining electrons from the cathode and accelerate electrons to be collected by the anode. The voltage drop at the cathode-fall region is usually between 8 and 12 V, and the voltage drop at the anode is reported to be 1−12 V.[33] Based on this structure, the arc voltage could be expressed as: $U_{arc} = U_{fall} + E_{col} \times l$, where U_{fall} represents the sum of anode- and cathode-fall voltages and E_{col} and l are, respectively, the electric field and length of the arc column. Before the LM bridge breakup occurs ($U_{arc} = 0$), there exists a stable initial current ($U_c = RI$ and $dI/dt = 0$). When the bridge pinches off and an arc is ignited, dI/dt must have a negative value equal to $-U_{arc}/L$, and thus the current I starts to decrease. Elongating the arc column length l guarantees an upward tendency of U_{arc}, and consequently, the current decreases. The faster the arc column is elongated, the more rapidly the current decreases.

On the other hand, the arc behavior during current interruption is also controlled by an energy model, which is simply depicted in Figure 1d that the energy input into an electrical arc is balanced by the radial thermal losses and radiation.[33] Theoretically, it is given as

$$\gamma E_{col}^2 = -\frac{1}{r}\frac{d}{dr}\left(r\lambda\frac{dT}{dr}\right) + P_r \quad (4)$$

where r is the arc radius, λ is the thermal conductivity, T is the temperature of the arc column, P_r is the radiation loss, and γ is the electrical conductivity of the arc plasma. With the arc column being elongated faster and longer, it is reasonable to expect that the arc energy dissipation (two terms on the right of eq 4) will be enhanced due to more intense interaction with the surrounding. As a result, E_{col} will consequently be strengthened, leading to an increase in arc voltage and a drop in current. At the initial stage, a slightly declined current is still able to maintain a high electrical conductivity γ via

https://doi.org/10.1021/acsaelm.2c00352
ACS Appl. Electron. Mater. 2022, 4, 2859−2868

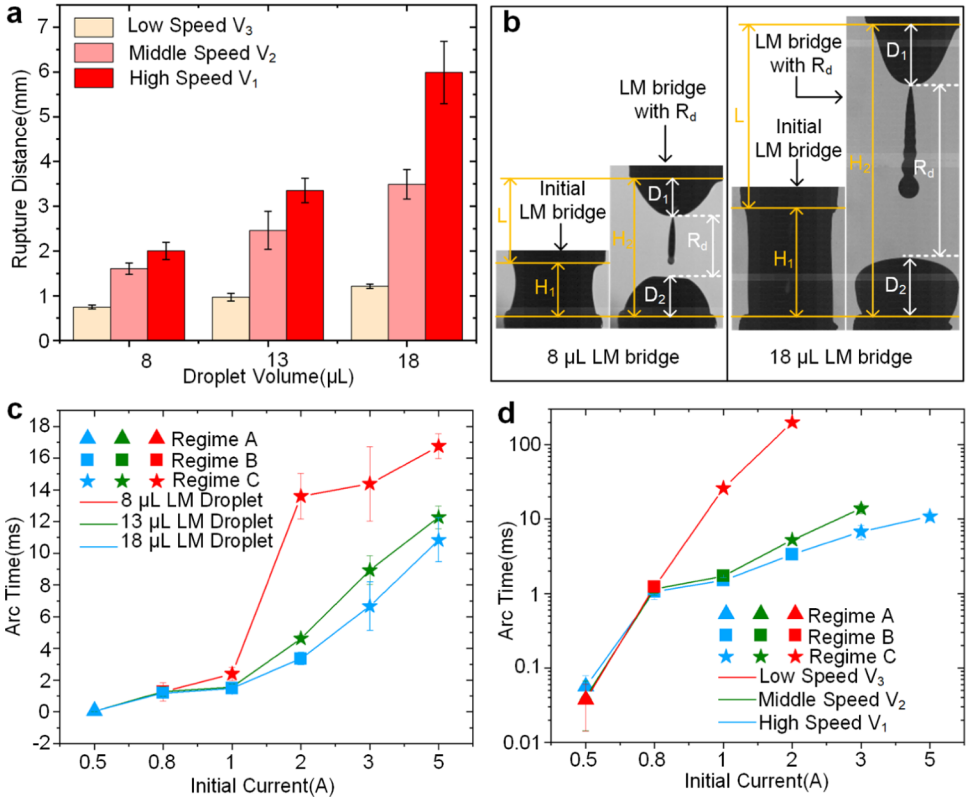

Figure 3. Control of LM bridge switch's arc time by LM volume and stretching velocity. (a) Rupture distance variations with LM volume and stretching velocity. Every rupture distance is averaged by all experimental results under the same parameters, and the error bars represent the standard deviation. (b) Comparison of the development of R_d in two LM bridges of different volumes, 8 and 18 μL, respectively. (c) Arc time as a function of the initial current, with LM bridge of different volumes. All LM bridges are stretched at a high speed V_1. The three regimes under the corresponding initial current are distinguished by different symbols. (d) Arc time as a function of the initial current with an 18 μL LM bridge at different stretching velocities. The three regimes under the same initial current are distinguished by different symbols. For (c) and (d), every arc time is averaged by three consecutive experimental results under the same parameters and the error bars represent the standard deviation.

persistent ionization. As the current decreases and energy dissipation goes on, sufficient plasma could not be fed by the circuit to hold a sufficient γ. Therefore, the current will finally be interrupted. The classical explanation of arc interruption principle indicates that the speed of arc column elongation plays an essential role in the current interruption process. The working mechanism schematic given in Figure 1d indicates that the arc generated in the LM bridge switch could be stretched at a higher speed. Compared to the solid-contact switch, it excels due to an extra stretching speed V_c originated from the surface tension-driven contraction of the LM filament. Apart from this, it is also interesting to note in Figure 1c that the ratio of the solid contact's arc time to that of the LM switch experiences a great fluctuation, which means that the performance superiority is not monolithically determined by the above factors.

To clarify the fluctuation of the LM switch's performance, we give deeper insights into the switch's working process by combining electrical measurements with high-speed imaging. We find that electrical arcs produced in the LM switch demonstrate three distinct regimes, which are summarized in Figure 2. Regime A (Movie S2) is characterized by a single arc burning, as shown in Figure 2a,b. Before the LM bridge breakup occurs (t_1−1 ms), an initial current of 0.5 A flows through the LM contact, causing a negligible voltage drop across the bridge thanks to the excellent electrical conductivity of Galinstan. At t_1, the filament pinches off and the electrical arc is ignited. Correspondingly, a 17 V drop in voltage between the cathode and anode is observed and the current is limited at 0.47 A. As the filament contracts further, the arc plasma continues to burn for 50 μs, and eventually the current is turned off at t_2.

Figure 2c,2d depicts arc plasma behaviors with voltage and current variations at an intermediate level of current (from 0.5 to 1 A), which we designate as regime B (Movie S3). After cathode-fall and anode-fall voltages are built at t_1, the circuit current drops to 0.95 A from 1 A. As the filament contracts under the action of surface tension, the electrical arc is stretched longer between the filament end and lower droplet; hence, the current keeps decreasing at t_2. At t_3, the filament pinches off at the upper end, generating another separated arc and a second pair of anode- and cathode-fall voltages. The instantaneous voltage drop causes a steep fall of ~0.05 A of current. Subsequently, the two arc columns are elongated concurrently due to the shrinkage of the middle filament to limit circuit current. At t_5, the current is too low to provide enough source of plasma to maintain arc burning. Thus, the current is chopped at 0.44 A to complete circuit interruption. In this regime, both the birth of the second pair of polar voltage and the contraction of the filament contribute to an elevated performance in current interruption. Interestingly, during the capillary breakup process, the LM filament may be disintegrated into several satellite droplets (Figure 2c, t_5 + 2 ms) due to the Rayleigh instabilities.[34] In this situation, if the

https://doi.org/10.1021/acsaelm.2c00352
ACS Appl. Electron. Mater. 2022, 4, 2859−2868

electrical arc is not interrupted and n satellite droplets are produced, there will be $n + 1$ pairs of anode-fall, cathode-fall voltages and n extra V_c built in the arc stretching process (see Figure S8), which is much more beneficial to the arc interruption performance.

At a larger current of 3 A, elongation of the two electrical arcs connected in series could not interrupt the circuit (Figure 2e2,f). When the filament contracts to a short enough length, which we define as the "leap distance" (L_d) (Figure 2e, t_5), plasma spread from the two tips of the filament will encounter to combine. Soon after the whole filament will be surrounded by plasma. At this point, the two independent arc columns leap across the filament and merge into a new one. The formation of the new coalesced arc column means the elimination of a pair of cathode-fall and anode-fall voltages. Note that a slight downhill slope appears on the voltage waveform and a slight uphill one emerges on the current waveform between t_4 and t_5 (Figure 2f). Upon the shrinkage of the filament, the newly formed arc column continues to be stretched by the electromechanical device to limit the current (Figure 2e, t_6). At t_7, the electrical arc extinguishes and the circuit current is chopped off at 0.48 A, and we define this as regime C (Movie S4). In this regime, the disappearance of an anode-fall voltage and a cathode-fall voltage as well as the elimination of the extra arc stretching contributed by the filament result in a drop in the current interruption performance. Another notable feature is the chop current and the chop voltage at the point of circuit interruption. We mark them on current and voltage waveforms in Figure 2 and give analysis in Supporting information Figure S9.

As a reference, arc resistance variations in the three regimes are also extracted and discussed in Figure S10 according to He et al.'s work.[24] To evaluate the influence of electrical arc on the Galinstan, we calculate the energy put into the electrical arc in three cases shown in Figure 2. Based on the U−I data recorded by the oscilloscope and $Q = \int_0^t UI\,dt$, the totally input arc energy is calculated to be 4.335 e^{-4} J, 7.19 e^{-2} J, and 0.78 J, respectively, corresponding to regime A, regime B, and regime C. With such a huge difference between arc energy, it indicates that there must be a significant temperature difference across the LM filament in three regimes and the regime C had better be averted. We further conducted experiments to examine the repeatability of the switch, as shown in Figure S11. We can see that the repeatability of the current interruption process mainly depends on the arc column stretching process, which is driven by the external mechanism and the LM filament contraction. The movement of the electromagnetic mechanism is stable, and the LM filament contraction is decided by the stability of its surface tension, which is also stable in an inert gas environment. Therefore, the LM switch shows high repeatability.

Next, a series of control experiments are conducted to further explore the LM bridge's current interruption characteristics. Three different sizes of LM bridges are constructed, respectively, with 8, 13, and 18 μL of Galinstan. We stretch every LM bridge with the three stretching velocities (V_1−V_3) to break a range of initial currents from 0.5 to 5 A and record every arc interruption process. Rupture distance variations with respect to bridge volumes and stretching velocities are plotted in Figure 3a. Figure 3b illustrates the development of a rupture distance (R_d) into two LM bridges using Galinstan droplets of different volumes (8 and 18 μL). At the point of rupture, R_d could be calculated as

$$R_d = H_2 - (D_1 + D_2) = (H_1 + L) - (D_1 + D_2) \quad (5)$$

Here, H_1 and H_2 are, respectively, the heights of the bridge at the initial state and at the R_d formation point, respectively; D_1 and D_2 represent the heights of two main droplets at the R_d formation point, respectively; and L is measured from two vertical positions of the upper LM bridge/solid electrode boundary, which represents the distance the LM bridge is extended to realize the second filament pinch-off. For two LM bridges of different volumes, the larger one will have both a higher H_1 and $(D_1 + D_2)$, which counteract and compromise in attribution to the calculation of R_d. On the other hand, a larger volume also means the bridge has a higher deformation tolerance towards the external vertical extension. As a result, the LM bridge with a larger volume must be stretched to a higher height to induce a high enough curvature and Laplace pressure for self-driving pinch-off. As can be seen, L of the 18 μL bridge is more than twice that of the 8 μL bridge. That explains why a larger volume leads to a higher R_d. For the LM bridge of a selected volume, Figure 3a indicates that the same LM bridge could pinch off with distinct rupture distances under different stretching velocities. For the stretching-induced capillary breakup of an LM bridge, three main factors are involved to determine the process. One is the surface tension, which exerts a Laplace pressure on a necked point as a self-driving source for the bridge rupture. The other two are gravity of the liquid and the stretching effect. The former tends to help the driving force pinch off the bridge at the lower end, and the latter resists the tendency as a stabilizing factor. As reported,[35] the stretching effect is characterized by a dimensionless velocity $U = (\rho R u^2/\sigma)^{1/2}$, where u is the stretching velocity. The overall trend of rupture distance that increases with the stretching velocity is due to the stabilizing effect of the increased inertial force over surface tension, which is measured by the Weber number U^2.[35]

Based on the above explanations, we know that varying the LM bridge volumes and stretching velocities could tune the rupture distance and finally the current interruption ability of the switch. As shown in Figure 3c,d, in which a larger-volume LM bridge and a higher stretching velocity help shorten the arc time under the same initial current. This part implies that the rupture distance formed during the breakup process is critical to control the current interruption performance of the LM switch. In addition, it is notable in Figure 3c,3d that the transition of the arc regime is influenced in some way. It seems that the transition from regime B to regime C is delayed in LM bridges with a larger rupture distance, which is caused by increased volume or stretching speed, as discussed later.

Apart from bridge volumes and stretching velocities, the dependence of rupture distance R_d on the electrode diameter R is also studied. Zhuang et al.'s work[35] has demonstrated that the rupture distance is mainly dependent on the Ohnesorge number $Oh = \mu/\sqrt{\rho R\sigma}$ and the dimensionless stretching velocity $U = \sqrt{\rho R u^2/\sigma}$. Here, μ is the viscosity of the liquid material. Obviously, the radius of the electrode area R influences both Oh and U. That is, the dependence of the rupture distance on the electrode area is very complicated and not monotonic. Apart from the electrode area, a bigger range of stretching velocities will lead to other intriguing characteristics, which also influence the arc behavior in bridge breakup, such as the transition of the rupture position and filament/thread shape change.[35] Detailed discussion and key simulation

https://doi.org/10.1021/acsaelm.2c00352
ACS Appl. Electron. Mater. 2022, 4, 2859−2868

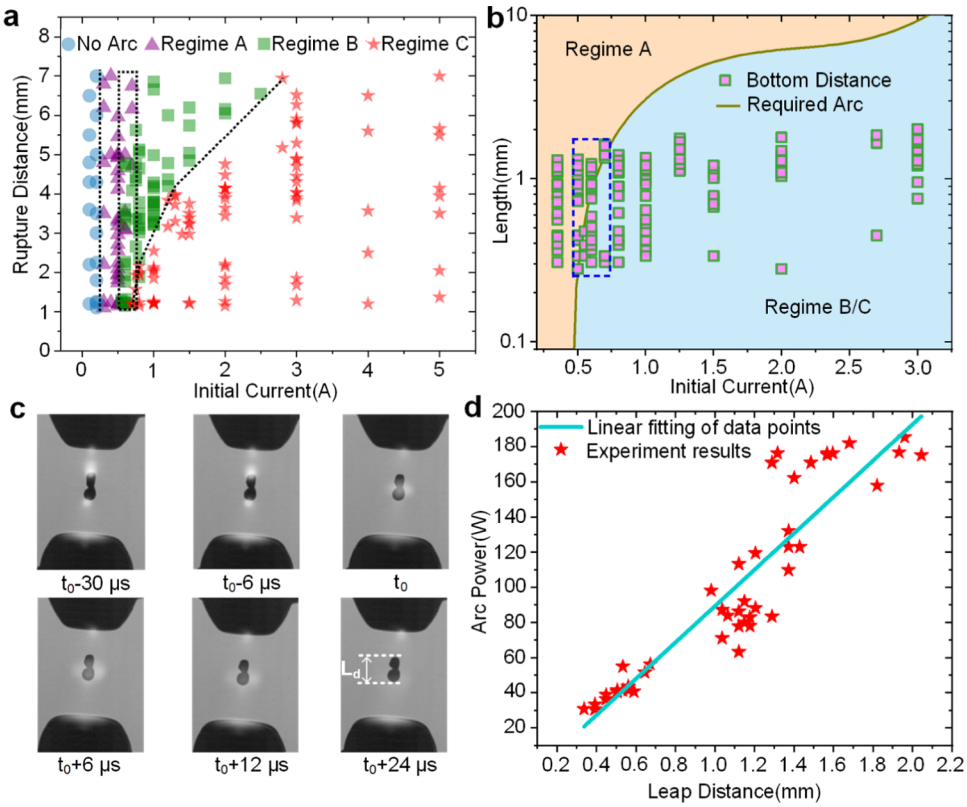

Figure 4. Regime transitions and regulations of electrical arcs. (a) Electrical arc phase diagram for LM bridges with different rupture distances subject to initial currents. Regime boundaries are marked by dotted lines. (b) Bottom distances versus initial currents, measured from all experimental trials. Fitted curve of required arc length as a function of initial currents is also plotted as a reference for regimes distinguished. (c) Close-up of the process of coalescence of two arc columns. The time t_0 is set at the first instant captured by the high-speed camera when two arc columns encounter. (d) Instantaneous arc power versus leap distance at the time of coalescence of two arcs. Every red star corresponds to one experiment trial controlled by arc in regime C.

results are given in Figure S12, in which numerical modeling was conducted to assist the investigation.

To investigate arc regime transitions, we stretch LM bridges of different volumes using a larger range of velocities. In Figure 4a, we give an electrical arc phase diagram as a function of initial current and rupture distance, with each data point representing the regime characterization of a single trial. For each value of a rupture distance, there is a progression from regime A to regime B and then regime C as the initial current increases. For completeness, we also probe the critical current value for arc generation. The phase boundary between the area without arc and regime A seems vertical, as the arc generation arises solely from the required minimum amount of energy input, which is 0.2 A in our case and is independent of the rupture distance.

The difference between regime A and regime B lies in whether an electrical arc could interrupt the circuit before the second pinch-off point appears. Therefore, the boundary distinguishing regime A and regime B relies on the competition between the bottom distance D_b and the required arc length for realizing the interruption of an initial current. After analyzing all experimental results, we find that the demanded arc length for interrupting a selected initial current is almost invariable (see Supporting information Figure S13). During the bridge breakup process, D_b, as we define in Figure 1c, represents the longest distance that could be developed between the filament end and the lower primary droplet before the upper end pinches. It is also equivalent to the biggest arc length that could be built in regime A. Therefore, the boundary initial current is located where the corresponding required arc length is equal to the bottom distance. If D_b is higher than the required arc length, the electrical arc will extinct before the second breakpoint appears, and it results in regime A. Otherwise, regime B takes over as the second arc emerges from the second break.

All experimental trials plotted in Figure 4a are picked up to measure the variation in D_b at different initial currents, as shown in Figure 4b. For multiple experiments conducted at the same initial current, we stretch LM bridges of different volumes with various speeds and D_b fluctuates in a small range between 0.28 and 2 mm. It seems that there is no clear rule between the D_b and R_d (see Supporting information Figure S14 for the variations of D_b versus R_d). Comparing D_b with the fitted curve of required arc length as a function of initial currents, we could figure out whether the electrical arc is in regime A or not. As marked in Figure 4b, when the initial current is lower than 0.5 A, D_b is always larger than the required arc length so that the LM switch works in regime A. In contrast, when the initial current increases to higher than 0.75 A, D_b is at a disadvantage, thus the electrical arc is operated in regime B or C. For an initial current of 0.5−0.75 A, the required arc length is in between the maximum and minimum of D_b. That is, under our experimental conditions, the regime of arcs to interrupt an initial current between 0.5 and 0.75 A is uncertain. So, the boundary between regime A and regime B is rather blurred, as is framed in Figure 4a,4b.

https://doi.org/10.1021/acsaelm.2c00352
ACS Appl. Electron. Mater. 2022, 4, 2859−2868

To understand the aggressive progression on the boundary between regime B and regime C, we focus on the process of coalescence of two arc columns, through which the transition from regime B to regime C is achieved. Figure 4c gives a close-up of two arc columns' merging, from which we can grasp critical factors dominating the process. Before t_0, two arc columns stagnate on two tips of the filament. At t_0, spread plasma from upper and lower tips encounters and results in a light plasma halo at the middle of the filament. The halo first expands (t_0 + 6 μs), then contracts (t_0 + 12 μs), and finally disappears (t_0 + 24 μs), indicating the formation of a whole new arc column. Considering that the plasma from two arc columns is driven to leap across a filament to combine, we surmise that the energy input into the two arcs plays an important role in spreading plasma and expanding the plasma halo. In Figure 4d, the instantaneous arc power at the instant of two arcs merging as a function of the leap distance is plotted. As the driving source for plasma spreading, the arc power is linearly proportional to the leap distance. A larger leap distance is based on a longer rupture distance developed in advance. For an LM bridge with a longer rupture distance, a larger arc power from a higher initial current is required to drive two arc columns to leap across a longer filament. As a result, the boundary between regime B and regime C progresses on initial currents with the increase of rupture distance. Therefore, controlling the bottom distance and the rupture distance developed in a capillary breakup process is an effective way to regulate arc regime transitions.

3. CONCLUSIONS

In summary, this paper has demonstrated basic operations, fundamental principles, and performance characteristics of a liquid-metal bridge-enabled switch for electrical power applications. According to the behaviors of electrical arcs developed in the capillary breakup of an LM bridge, three arc regimes are identified to characterize the device's switch-off process. The three arc regimes correlate closely to the switch's working performance. When functioning in regime B, where two separated arcs cooperate to limit a current, the LM switch exceeds a traditional solid switch in interruption speed by a factor of up to 20. Regulations of arc regime transitions and current interruption performance are mainly determined by the rupture distance formed in a capillary breakup process, which could be tuned by varying the LM bridge volumes and stretching velocities. Endowed with a superior arc interruption ability and self-healing liquid-metal contacts, the LM bridge switch could be integrated into soft systems and has a great potential to achieve high-power, stretchable, yet long-lifetime electrical equipment. In addition, the unprecedented, intriguing phenomena arising from the interactions between electrical arc and liquid bridge capillary breakup may illuminate certain fundamental research in fluid dynamics and plasma science. The use of a glovebox and the existence of electrical feedthroughs indeed restrict the use of the proposed switch in real-world scenarios. However, this problem can be solved by encapsulating the LM bridge in a compact tube filled with inert gas, which is subjected to our future investigation. The application of an LM bridge in a transient high-current occasion also looks promising.[36] Based on the controllable production of liquid metal droplets and their control actuation in microfluidic channels,[37,38] it is possible to miniaturize the presented electrical switch to fabricate micro-sized switch arrays that can be integrated into lab-on-a-chip platforms.

4. EXPERIMENTAL SECTION

4.1. Materials. Galinstan used in experiments was purchased from Sigma-Aldrich (GF98079777-1EA). Deposition and volume control of LM droplets are realized utilizing a precise pipette (Gilson P20N).

4.2. Glovebox System. The glovebox is tailor-made by Mikrouna (China) with oxygen and moisture sensors. It offers an inert environment (nitrogen) with an oxygen content lower than 0.01 ppm (parts per million). Coaxial adapters and aviation plugs are installed on the box wall to transmit signals.

4.3. Electrical Measurement. The outside DC power supply maintains a constant 220 V with a variable resistor to adjust the current. The total length of the conducting wire is less than 1.5 m, which means the stray inductance could almost be neglected at such a low-frequency circuit. A differential voltage probe (Tektronix THDP 0200) and a current probe (Tektronix TCP0030A) are, respectively, used to acquire voltage and current variations of the LM bridge during the switch-off process. Voltage and current waveforms are recorded in an oscilloscope (Tektronix MDO3104).

4.4. High-Speed Visualization. A transparent observation window is reserved on the glovebox wall to help visualize the behaviors of an LM bridge. The high-speed images of the breakup process of LM bridges are captured by a high-speed camera (Phantom V2012, Vision Research, Inc.) fitted with a MACRO-NIKKOR 65 mm lens, and the magnification of the lens is set at 1×. A blue LED parallel light source is placed behind the LM bridge to provide a back illumination for the shadowgraph setup.

■ ASSOCIATED CONTENT

Supporting Information

The Supporting Information is available free of charge at https://pubs.acs.org/doi/10.1021/acsaelm.2c00352.

Schematic of the switch prototype and the entire experimental system; validation of the oxygen-free environment in the glove box; surface tension measurement of Galinstan; motion characteristics of the upper electrode; driving currents of the mechanisms; voltage and current waveforms of a 220 V to 0.1 A interruption by LM switch; Comparison of two simulated bridge breakup processes, (a) without and (b) with a satellite droplet; stretching an oxidized LM bridge to interrupt a 220 V^{-1} A circuit; image sequences of the LM bridge and electrical arc; current and voltage waveforms; current interruption waveforms of the solid-contact switch, under different parameters; expected arc behaviours with two separated LM droplets in between; modeling analysis of chop currents and chop voltages; chop current variations versus initial currents; schematic diagram of the experimental circuit with arc burning; model predicted and experimentally determined chop voltages as a function of initial currents; current and arc resistance variations in three arc regimes; repeatability test of the LM switch; dependence of Rd on the electrode area R; Ld as a function of the stretching velocity U for liquid bridges with different Oh; Ld as a function of U; breakup process of 8 μL LM bridges with different areas, stretched at a 0.2m/s uniform velocity; required total arc length as a function of the initial current; variations of bottom distance versus rupture distance (PDF)

Stretching a liquid-metal bridge to interrupt a 0.1 A current (MP4)

Stretching a liquid-metal bridge to interrupt a 0.5 A current (MP4)

Stretching a liquid-metal bridge to interrupt a 1 A current (MP4)

https://doi.org/10.1021/acsaelm.2c00352
ACS Appl. Electron. Mater. 2022, 4, 2859−2868

Stretching a liquid-metal bridge to interrupt a 3 A current (MP4)

AUTHOR INFORMATION

Corresponding Authors

Fei Yang − *State Key Laboratory of Electrical Insulation and Power Equipment, School of Electrical Engineering, Xi'an Jiaotong University, Xi'an 710049, China*; Email: yfei2007@mail.xjtu.edu.cn

Shi-Yang Tang − *Department of Electronic, Electrical and Systems Engineering, University of Birmingham, Birmingham B15 2TT, U.K.*; orcid.org/0000-0002-3079-8880; Email: S.Tang@bham.ac.uk

Mingzhe Rong − *State Key Laboratory of Electrical Insulation and Power Equipment, School of Electrical Engineering, Xi'an Jiaotong University, Xi'an 710049, China*; Email: mzrong@xjtu.edu.cn

Authors

Xiaonan Zhu − *State Key Laboratory of Electrical Insulation and Power Equipment, School of Electrical Engineering, Xi'an Jiaotong University, Xi'an 710049, China*

Haoran Wang − *State Key Laboratory of Electrical Insulation and Power Equipment, School of Electrical Engineering, Xi'an Jiaotong University, Xi'an 710049, China*

Siyuan Zhao − *State Key Laboratory of Electrical Insulation and Power Equipment, School of Electrical Engineering, Xi'an Jiaotong University, Xi'an 710049, China*

Yi Wu − *State Key Laboratory of Electrical Insulation and Power Equipment, School of Electrical Engineering, Xi'an Jiaotong University, Xi'an 710049, China*

Complete contact information is available at: https://pubs.acs.org/10.1021/acsaelm.2c00352

Author Contributions

The manuscript was written through contributions of all authors. All authors have given approval to the final version of the manuscript.

Notes

The authors declare no competing financial interest.

ACKNOWLEDGMENTS

This research was supported by the National Natural Science Foundation under nos. U1966602 and 52077172; the Research Program of Shaanxi Province under no. 2019ZDLGY18-05; and the Shaanxi Province "Sanqin scholars" innovation team project (Demonstration innovation team of XJTU for the key technology of advanced DC power equipment and its industrialization).

ABBREVIATIONS

LM, liquid metal; R_d, rupture distance; D_b, bottom distance

REFERENCES

(1) Dickey, M. D. Stretchable and Soft Electronics using Liquid Metals. *Adv. Mater.* **2017**, *29*, No. 1606425.

(2) Barbee, M. H.; Mondal, K.; Deng, J. Z.; Bharambe, V.; Neumann, T. V.; Adams, J. J.; Boechler, N.; Dickey, M. D.; Craig, S. L. Mechanochromic Stretchable Electronics. *ACS Appl. Mater. Interfaces* **2018**, *10*, 29918−29924.

(3) Barron, E. J.; Peterson, R. S.; Lazarus, N.; Bartlett, M. D. Mechanically Cloaked Multiphase Magnetic Elastomer Soft Composites for Wearable Wireless Power Transfer. *ACS Appl. Mater. Interfaces* **2020**, *12*, 50909−50917.

(4) Sun, J.; Pu, X.; Liu, M.; Yu, A.; Du, C.; Zhai, J.; Hu, W.; Wang, Z. L. Self-Healable, Stretchable, Transparent Triboelectric Nanogenerators as Soft Power Sources. *ACS Nano* **2018**, *12*, 6147−6155.

(5) Shu, J.; Ge, D. A.; Wang, E.; Ren, H.; Cole, T.; Tang, S. Y.; Li, X.; Zhou, X.; Li, R.; Jin, H.; Li, W.; Dickey, M. D.; Zhang, S. A Liquid Metal Artificial Muscle. *Adv. Mater.* **2021**, *33*, No. e2103062.

(6) Khan, Y.; Ostfeld, A. E.; Lochner, C. M.; Pierre, A.; Arias, A. C. Monitoring of Vital Signs with Flexible and Wearable Medical Devices. *Adv. Mater.* **2016**, *28*, 4373−4395.

(7) Sen, P.; Kim, C.-J. C. J. Microscale Liquid-Metal Switches—A Review. *IEEE Trans. Ind. Electron.* **2009**, *56*, 1314−1330.

(8) Chen, W.; Zeng, R.; He, J.; Wu, Y.; Wei, X.; Fang, T.; Yu, Z.; Yuan, Z.; Wu, Y.; Zhou, W.; Yang, B.; Qu, L. Development and prospect of direct-current circuit breaker in China. *High Voltage* **2021**, *6*, 1−15.

(9) Gui, Q.; He, Y.; Wang, Y. Soft Electronics Based on Liquid Conductors. *Adv. Electron. Mater.* **2020**, *7*, No. 2000780.

(10) Khan, M. R.; Trlica, C.; So, J. H.; Valeri, M.; Dickey, M. D. Influence of water on the interfacial behavior of gallium liquid metal alloys. *ACS Appl. Mater. Interfaces* **2014**, *6*, 22467−22473.

(11) Ray, N.; Kempf, B.; Mutzel, T.; Heringhaus, F.; Froyen, L.; Vanmeensel, K.; Vleugels, J. Effect of Ni addition on the contact resistance of Ag-WC electrical contacts. *J. Alloy Compd.* **2016**, *670*, 188−197.

(12) Ren, W.; Du, D.; Du, Y. Electrical Contact Resistance of Connector Response to Mechanical Vibration Environment. *IEEE Trans. Compon., Packag., Manuf. Technol.* **2020**, *10*, 212−219.

(13) Ren, W.; Wang, P.; Fu, Y.; Pan, C.; Song, J. Effects of temperature on fretting corrosion behaviors of gold-plated copper alloy electrical contacts. *Tribol. Int.* **2015**, *83*, 1−11.

(14) Bose, B. K. Power Electronics-A Technology Review. *Proc. IEEE* **1992**, *80*, 1303−1334.

(15) Wang, L.; McCarthy, T. J. Capillary-bridge-derived particles with negative Gaussian curvature. *Proc. Natl. Acad. Sci. U.S.A.* **2015**, *112*, 2664−2669.

(16) Wang, L.; Qiu, M.; Yang, Q.; Li, Y.; Huang, G.; Lin, M.; Lu, T. J.; Xu, F. Fabrication of Microscale Hydrogels with Tailored Microstructures based on Liquid Bridge Phenomenon. *ACS Appl. Mater. Interfaces* **2015**, *7*, 11134−11140.

(17) Fuller, S. B.; Wilhelm, E. J.; Jacobson, J. M. Ink-jet printed nanoparticle microelectromechanical systems. *J. Microelectromech. Syst.* **2002**, *11*, 54−60.

(18) Vogel, M. J.; Steen, P. H. Capillarity-based switchable adhesion. *Proc. Natl. Acad. Sci. U.S.A.* **2010**, *107*, 3377−3381.

(19) Hu, B.; Xue, L.; Yang, P.; Han, Y. Variable-focus liquid microlenses with adjustable 3-D curved housings. *Langmuir* **2010**, *26*, 6350−6356.

(20) Eaker, C. B.; Hight, D. C.; O'Regan, J. D.; Dickey, M. D.; Daniels, K. E. Oxidation-Mediated Fingering in Liquid Metals. *Phys. Rev. Lett.* **2017**, *119*, No. 174502.

(21) Morley, N. B.; Burris, J.; Cadwallader, L. C.; Nornberg, M. D. GaInSn usage in the research laboratory. *Rev. Sci. Instrum.* **2008**, *79*, No. 056107.

(22) Wissman, J.; Dickey, M. D.; Majidi, C. Field-Controlled Electrical Switch with Liquid Metal. *Adv. Sci.* **2017**, *4*, No. 1700169.

(23) He, H.; Wu, Y.; Niu, C.; Yang, Z.; Rong, M.; Sun, Y.; Li, K. Investigation of the Pinch Mechanism of Liquid Metal for the Current Limitation Application. *IEEE Trans. Compon., Packag., Manuf. Technol.* **2017**, *7*, 563−571.

(24) He, H.; Wu, Y.; Yang, Z.; Zhao, P.; Zhu, X.; Niu, C.; Rong, M. Study of Liquid Metal Fault Current Limiter for Medium-Voltage DC Power Systems. *IEEE Trans. Compon., Packag., Manuf. Technol.* **2018**, *8*, 1391−1400.

(25) Tang, S. Y.; Khoshmanesh, K.; Sivan, V.; Petersen, P.; O'Mullane, A. P.; Abbott, D.; Mitchell, A.; Kalantar-Zadeh, K. Liquid metal enabled pump. *Proc. Natl. Acad. Sci. U.S.A.* **2014**, *111*, 3304−3309.

(26) Bezdenejnykh, N. A.; Meseguer, J.; Perales, J. M. Experimental analysis of stability limits of capillary liquid bridges. *Phys. Fluids A* **1992**, *4*, 677−680.
(27) Liu, T.; Sen, P.; Kim, C.-J. Characterization of Nontoxic Liquid-Metal Alloy Galinstan for Applications in Microdevices. *J. Microelectromech. Syst.* **2012**, *21*, 443−450.
(28) Handschuh-Wang, S.; Chen, Y. Z.; Zhu, L. F.; Zhou, X. C. Analysis and Transformations of Room-Temperature Liquid Metal Interfaces - A Closer Look through Interfacial Tension. *Chemphyschem* **2018**, *19*, 1584−1592.
(29) Ladd, C.; So, J. H.; Muth, J.; Dickey, M. D. 3D printing of free standing liquid metal microstructures. *Adv. Mater.* **2013**, *25*, 5081−5085.
(30) Xu, Q.; Oudalov, N.; Guo, Q. T.; Jaeger, H. M.; Brown, E. Effect of oxidation on the mechanical properties of liquid gallium and eutectic gallium-indium. *Phys. Fluids* **2012**, *24*, No. 063101.
(31) Eggers, J.; Villermaux, E. Physics of liquid jets. *Rep. Prog. Phys.* **2008**, *71*, No. 036601.
(32) Castrejón-Pita, J. R.; Castrejon-Pita, A. A.; Thete, S. S.; Sambath, K.; Hutchings, I. M.; Hinch, J.; Lister, J. R.; Basaran, O. A. Plethora of transitions during breakup of liquid filaments. *Proc. Natl. Acad. Sci. U.S.A.* **2015**, *112*, 4582−4587.
(33) Slade, P. G. *Electrical Contacts: Principles and Applications*; Crc Press Taylor & Francis Group, 2017; pp 578−581.
(34) Rayleigh, L. On The Instability Of Jets. *Proc. London Math. Soc.* **1878**, *s1−10*, 4−13.
(35) Zhuang, J.; Ju, Y. S. A Combined Experimental and Numerical Modeling Study of the Deformation and Rupture of Axisymmetric Liquid Bridges under Coaxial Stretching. *Langmuir* **2015**, *31*, 10173−10182.
(36) Zhu, X.; Yang, F.; Wang, H.; Zhao, S.; Wu, Y.; Wu, Y.; Rong, M. Robust electrical contacts integrating a liquid metal bridge for mechanical switches. *J. Phys. D: Appl. Phys.* **2022**, *55*, No. 145002.
(37) Tang, S. Y.; Joshipura, I. D.; Lin, Y.; Kalantar-Zadeh, K.; Mitchell, A.; Khoshmanesh, K.; Dickey, M. D. Liquid-Metal Microdroplets Formed Dynamically with Electrical Control of Size and Rate. *Adv. Mater.* **2016**, *28*, 604−609.
(38) Khoshmanesh, K.; Tang, S. Y.; Zhu, J. Y.; Schaefer, S.; Mitchell, A.; Kalantar-Zadeh, K.; Dickey, M. D. Liquid metal enabled microfluidics. *Lab Chip* **2017**, *17*, 974−993.

https://doi.org/10.1021/acsaelm.2c00352
ACS Appl. Electron. Mater. 2022, 4, 2859−2868